Wim van Westrenen · Bernard J. Wood
Jonathan D. Blundy

A predictive thermodynamic model of garnet–melt trace element partitioning

Abstract We have developed a predictive model for the partitioning of magnesium and a range of trivalent trace elements (rare earth elements, Y, In and Sc) between garnet and anhydrous silicate melt as a function of pressure, temperature and bulk composition. The model for the magnesium partition coefficient, D_{Mg}, is based on a thermodynamic description of the pyrope ($\mathrm{Mg_3Al_2Si_3O_{12}}$) melting reaction between garnet and melt. Simple activity–composition relations, which take explicit account of garnet non-ideality, link D_{Mg} to the free energy of fusion (ΔG_f) of pure pyrope without the need to invoke non-ideality in the liquid phase. The resulting predictive equation, based on the compositions of a large set ($n=160$) of published garnet–melt pairs, produces values of D_{Mg} that are within 20% of measured values at temperatures between 1,450 and 1,930 °C, and pressures between 2.5 and 7.5 GPa. The model for trivalent ($3+$) trace elements is based on the lattice strain approach to partitioning, which describes mineral–melt partition coefficients in terms of three parameters: the effective radius, $r_0(3+)$, of the site on which partitioning takes place (in this case, the garnet X-site); the apparent site Young's modulus $E_X(3+)$; and the partition coefficient $D_0(3+)$ for a fictive trivalent element J^{3+}, with radius $r_0(3+)$, that does not strain the crystal lattice when entering the garnet X-site. Analogous to the model for D_{Mg}, simple activity–composition relations link $D_0(3+)$ to ΔG_f of a hypothetical garnet component incorporating a hypothetical rare earth element J^{3+} through a YAG-type charge-balancing mechanism ($\mathrm{J}^{3+}\mathrm{Mg_2Al_3Si_2O_{12}}$). Through analysis of existing garnet–melt rare earth element partitioning data ($n=18$ garnet–melt pairs), an expression is derived relating $D_0(3+)$ to pressure, temperature and D_{Mg}. Predicted $D_{\mathrm{REE/Y/Sc}}$ values agree to within 5–50% of experimental measurements for all elements except La and Ce, which are liable to large experimental errors, spanning pressures between 2.5 and 5.0 GPa and temperatures between 1,430 and 1,640 °C. In conjunction with our new parameterisation for D_{Mg}, and previously published equations linking $r_0(3+)$ and $E_X(3+)$ to garnet major element composition, this model gives a description of trivalent REE, Y, In and Sc partitioning between garnets and anhydrous melts over a range of pressures, temperatures and compositions relevant to melting of garnet-bearing sources in the Earth's upper mantle.

W. van Westrenen (✉) · B.J. Wood · J.D. Blundy
CETSEI, Department of Earth Sciences,
University of Bristol, Wills Memorial Building,
Queen's Road, Bristol BS8 1RJ, UK

Present address: W. van Westrenen
Geophysical Laboratory,
Carnegie Institution of Washington,
5251 Broad Branch Road NW,
Washington, DC 20015, USA
e-mail: w.van_westrenen@gl.ciw.edu
Tel.: +1-202-4788926, Fax: +1-202-4788901

Editorial responsibility: E.H. Hauri

Introduction

Partial melting in the Earth's mantle is a polybaric, polythermal process through which the compositions of melt and mineral phases vary continuously as functions of pressure (P) and temperature (T). These variations undoubtedly have an impact on mineral–melt trace element partitioning coefficients (D's), because D's are thermodynamic variables. Due to a lack of data, geochemists interested in developing models of trace element evolution during melting are usually forced to assume constant D's (e.g. Salters and Hart 1989; Spiegelman 1996; Putirka 1999). Only when quantitative, predictive partitioning models are developed for all minerals deemed important in mantle melting, can accurate modelling of petrogenetic processes be achieved.

There are two contrasting experimental approaches to acquiring a framework of partitioning data relevant to mantle melting. One is to measure D's in experiments designed to resemble as closely as possible the P–T

conditions and phase compositions at the mantle solidus (e.g. Blundy et al. 1998; Salters and Longhi 1999). This method can produce the most accurate set of partition coefficients applicable to mantle melting, provided consensus is reached concerning the physical and chemical boundary conditions at the mantle solidus. Unfortunately, mineral and melt compositions, and physical parameters of mantle melting at the solidus are hotly debated in the geochemical community (e.g. Baker et al. 1995; Falloon et al. 1997, 1999; Hirschmann et al. 1998; Robinson et al. 1998; Hirschmann 2000). A telling illustration of this problem is that although Blundy et al. (1998) and Salters and Longhi (1999) both claim to provide clinopyroxene–melt partition coefficients applicable to the beginning of melting on the spinel lherzolite solidus at 1.5 GPa, their experimental temperatures differ by up to 235 °C. As a result of temperature, pressure and compositional differences in their melts and crystals, cpx–melt D_{Lu} at the putative 1.5 GPa solidus is a factor of three lower in the Salters and Longhi (1999) study.

A second approach entails systematic experiments aimed at isolating the effects of temperature, pressure and composition on partitioning (e.g. Ray et al. 1983; Lundstrom et al. 1998; Van Westrenen et al. 1999a; Hill et al. 2000; Law et al. 2000). This method is not aimed at matching as closely as possible the conditions thought to be apt for the description of a specific petrogenetic model. Instead, the attempt is to disentangle the effects of P, T and X, in which case extrapolation becomes relatively straightforward. Furthermore, precise knowledge of the effects of P, T, and mineral and melt composition on partitioning offers insight into the fundamental physical and chemical processes that control mineral–melt partitioning. In a series of papers (Van Westrenen et al. 1999a, 2000b), we have developed parts of a predictive garnet–melt trace element partitioning model based on this second approach.

Garnet (general formula $X_3^{VIII}Y_2^{VI}Z_3^{IV}O_{12}$, roman numerals denote coordination number) is a key mineral in many petrogenetic models. It is invoked as a residual mineral in formation of komatiites (e.g. Ohtani et al. 1989; Herzberg and Zhang 1997), calc-alkaline volcanic rocks (e.g. Green and Ringwood 1968), and oceanic island basalts (e.g. Stracke et al. 1999 and references therein). Furthermore, the role of garnet during the initial melting beneath mid-ocean ridges is hotly debated (e.g. Salters and Hart 1989; Johnson et al. 1990; LaTourrette et al. 1993; Bourdon et al. 1996; Hirschmann and Stolper 1996; Wood et al. 1999; Turner et al. 2000). Clearly, a predictive model for element partitioning between garnets and silicate melts is important for meaningful petrogenetic modelling of melting in the presence of garnet. Key trace elements in this respect are the rare earth elements and the high field strength elements. Although we develop here a predictive model for the former, our methodology is, in principle, extendable to the latter (e.g. Van Westrenen et al. 2001).

The model we use to describe variations in garnet–melt D's was developed by Blundy and Wood (1994), and has been applied successfully to a parameterisation of clinopyroxene–melt partitioning of rare earth elements (Wood and Blundy 1997). The model is based on lattice strain theory (Brice 1975). In the case of garnet, it describes partitioning of a series of isovalent trace elements with radii r into the dodecahedral garnet X-site as a function of the effective size of the site, r_0, the apparent elasticity of the X-site site, E_X, and the maximum partition coefficient D_0 for a trace element of radius r_0. The partition coefficient of element i, D_i, is given by:
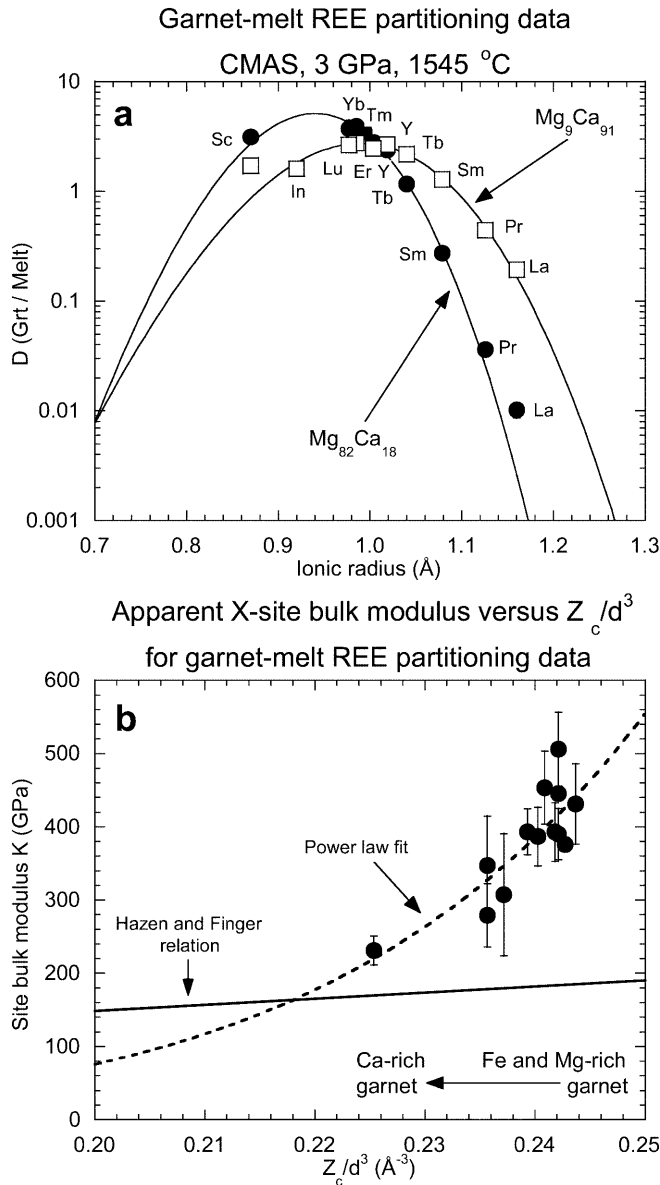
$$D_i^{Grt/Melt} = D_0^{Grt/Melt} \cdot \exp\left(\frac{-4\pi E_X N_A \left(\frac{r_0}{2}(r_i - r_0)^2 + \frac{1}{3}(r_i - r_0)^3\right)}{RT}\right)$$

(1)

Predicting D_i therefore requires linking r_0, E_X and D_0 to garnet and melt composition, P and T. In the next section, our earlier work on models for $r_0(3+)$ and $E_X(3+)$ is summarised, after which a model for $D_0(3+)$ is developed.

Prediction of r_0 and E_X

Predictive equations for $r_0(3+)$ and $E_X(3+)$ were derived in previously published studies (Van Westrenen et al. 1999a, 2000b). It has long been observed that r_0 is generally close to the size of the site on which partitioning takes place (e.g. Jensen 1973; Matsui et al. 1977; Philpotts 1978; Blundy and Wood 1994), implying a link between crystal chemistry and r_0. However, recent experimental studies have shown that r_0 decreases as a function of trace element charge (Van Westrenen et al. 1999a, 1999b, 2000b; Blundy and Dalton 2000; Law et al. 2000). For example, in garnet $r_0(3+)$ is consistently smaller than $r_0(2+)$ by around 0.05 Å (Van Westrenen et al. 1999b). This observation is confirmed by recent computer simulations of the energetics of garnet–melt partitioning (Van Westrenen et al. 2000a), which strongly suggest that r_0 in mineral–melt systems can vary considerably with trace element charge and cannot be assumed equal to the crystallographic size of the site on which partitioning takes place. The nature of this variation depends on both the crystal structure and the nature of the melt. Quantitative relations between r_0, E_X and crystal chemistry should therefore be derived from well-constrained systematic mineral–melt partitioning data and cannot be predicted accurately from crystal-structural data alone. To quantify this link for garnet we performed experiments in simple systems at constant P and T to isolate the effects of composition.

Figure 1a is a plot of D versus ionic radius for two experiments in the CMAS system at 3 GPa, 1,545 °C. Filled symbols are garnet–melt D values for the REE in Mg(Py)-rich garnet. The X-site of this garnet contains 82% Mg and 18% Ca. Open symbols are data for a Ca(Gr)-rich garnet (with 91% Ca and 9% Mg). The lines

Garnet-melt REE partitioning data
CMAS, 3 GPa, 1545 °C

Apparent X-site bulk modulus versus Z_c/d^3
for garnet-melt REE partitioning data

Fig. 1 Data used for derivation of predictive models for $r_0(3+)$ and $E_X(3+)$ for garnet–melt partitioning. **a** Shift to higher values of $r_0(3+)$ with increasing garnet Ca/(Ca+Mg) (Van Westrenen et al. 1999a). **b** Decrease in X-site modulus with increasing Ca/(Ca+Mg) (Van Westrenen et al. 2000b). 1σ errors shown when bigger than symbol

are fits to the data using the Blundy and Wood model [Eq. (1)]. $r_0(3+)$ clearly shifts as a function of composition. It is bigger for Gr-rich garnet than for Py-rich garnet, which is a result of the size difference between eight-fold coordinated Ca^{2+} ($r=1.12$ Å) and Mg^{2+} ($r=0.89$ Å) ions. As these experiments were performed near-isothermally and isobarically, $r_0(3+)$ values for end members Py and Gr can be derived by extrapolation. Using iron-bearing experiments performed at the same P and T, the effect of the almandine component could also be quantified (Van Westrenen et al. 2000b).

In the absence of systematic partitioning experiments, the effects of the other (minor) garnet X-site cations, and

the effect of changes in garnet Cr/Al ratio, were estimated from crystallographic data on the corresponding end members (e.g. the effect of Mn on $r_0(3+)$ was estimated from the X-site size of spessartine). To allow for a decrease in X-site radius with increasing pressure, a pressure correction term was added (for details see Van Westrenen et al. 2000b). In this way, we derived the following predictive model linking $r_0(3+)$ to garnet composition:

$$r_0(3+)[\text{Å}] = \mathbf{0.930} \cdot X_{Py} + \mathbf{0.993} \cdot X_{Gr} + \mathbf{0.916} \cdot X_{Alm} + 0.946 \cdot X_{Spes}$$
$$+ 1.05 \cdot (X_{And} + X_{Uv}) - \mathbf{0.005} \cdot (P[\text{GPa}] - 3.0)(\pm 0.005 \text{Å})$$
$$(2)$$

Bold values in Eq. (2) were derived from partitioning experiments (as in Fig. 1a); values in regular type from crystallographic data. A simple cation fraction approach was taken to obtain the X_i values in Eq. (2), e.g. $X_{Py} = Mg/(Mg + Ca + Fe^{2+} + Mn)$.

Previous work on clinopyroxene–melt and plagioclase–melt partitioning (Blundy and Wood 1994; Wood and Blundy 1997) showed a link between values of apparent Young's moduli E_X, taken from fits of experimental data to Eq. (1), and Young's moduli predicted using the bulk modulus–polyhedral volume relation of Hazen and Finger (1979). In Fig. 1b, fitted values of E_X for garnet–melt partitioning data are plotted against the volume of the X-site, divided by the charge of the cation on the X-site – in this case $3+$ for the REE. Ca-rich garnets plot towards the high-volume end of Fig. 1b, while the X-sites of Mg/Fe-rich garnets have relatively small volumes. There is a significant increase in the apparent site stiffness as the site volume decreases. In other words, it appears increasingly difficult to compress the X-site as its volume decreases. It is clear from Fig. 1b that fitted values of E_X deviate by up to a factor of two from the Hazen and Finger (1979) relation. Clearly, in the case of the garnet X-site, factors other than M–O bond compressibility must influence values of apparent E_X derived from partitioning studies.

Computer simulations elucidated one possible reason behind the apparent stiffness of the garnet X-site (Van Westrenen et al. 2000a). They show that the coordination number of both major and trace elements in the melt can influence the absolute value of the apparent site modulus E_X derived from partitioning data. A further possibility is that relatively small cation sites deform by distorting the coordinating tetrahedra and octahedra rather than by bulk compression. In the absence of a good theoretical model, however, an empirical approach is taken. A power law fit through the data gives the following expression, linking E_X to garnet composition:

$$E_X(3+)[\text{GPa}] = 3.5 \times 10^{12} \cdot (1.38 + r_0(3+)[\text{Å}])^{-26.7}(\pm 30 \text{GPa}) \quad (3)$$

Using Eqs. (2) and (3), knowledge of just one $D_{REE/Y/Sc}$, in conjunction with the garnet major element composition, P and T, is sufficient to predict $D^{Grt/Melt}$ for all other REE, Y and Sc to within 10–40% relative (Van Westrenen et al. 2000b).

Prediction of $D_0(3+)$: thermodynamics of garnet–melt partitioning

In order to render our model for the rare earth elements Y and Sc fully predictive, an expression must be found relating $D_0(3+)$ to P, T and melt compositions. We obtain this expression using thermodynamic analysis of garnet–melt equilibria. Our model for $D_0(3+)$ builds on a thermodynamic description of D_{Mg}, derived from the pyrope melting curve. The approach is analogous to that of Blundy et al. (1995), who derived a model for D_{Na} applicable to clinopyroxene–melt partitioning via analysis of the jadeite melting curve.

It has long been suggested that mineral melting curves (which describe the points in P–T space where mineral and melt of the same composition coexist) can be related to the activities of those minerals in multi-component silicate melts (e.g. Bowen 1913; Burnham 1981). Blundy et al. (1995) showed that, at a given pressure and temperature, the activities of the jadeite component ($NaAlSi_2O_6$) in clinopyroxene and coexisting *multi-component* melt bear a simple relationship to the standard state free energy change for the melting of *pure* jadeite at the same P and T. By converting the activities of jadeite into compositions, using a simple activity–composition relation, Blundy et al. (1995) linked the free energy change of jadeite melting at a given P and T to D_{Na} under the same conditions. D_{Na} could then be predicted as a function of P and T through the jadeite melting curve. Subsequently, Wood and Blundy (1997) showed similar links between the melting curve of diopside ($CaMgSi_2O_6$) and the partitioning of this component between clinopyroxene and melt.

The pyrope melting curve

The most abundant component found in natural magmatic garnets is the Mg end member, pyrope ($Mg_3Al_2Si_3O_{12}$). Let us therefore consider the pyrope fusion equilibrium:

$$Mg_3Al_2Si_3O_{12}(garnet) = Mg_3Al_2Si_3O_{12}(melt) \qquad (4)$$
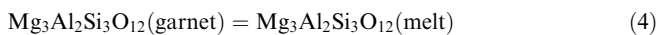
Taking the standard state to be pure $Mg_3Al_2Si_3O_{12}$ garnet and liquid at the P and T of interest, the standard state free energy change ΔG_f^0 for this reaction at P and T is given by:

$$\Delta G_{f(P,T)}^0 = \Delta H_{f(0.1,T_f)}^0 + \int_{T_f}^{T} \Delta C_P^0 dT$$
$$- T\left[\Delta S_{f(0.1,T_f)}^0 + \int_{T_f}^{T}\left(\frac{\Delta C_P^0}{T}\right)dT\right] + \int_{0.1MPa}^{P} \Delta V^0 dP \qquad (5)$$

where $\Delta H_{f(0.1,T_f)}^0$, ΔC_P^0, $\Delta S_{f(0.1,T_f)}^0$, and ΔV^0, denote differences in thermodynamic properties between pure pyrope melt and crystal at 0.1 MPa and T_f (the

(hypothetical) melting temperature of pure pyrope at 0.1 MPa). The integrals take account of differences in these properties between (0.1 MPa, T_f) and the P and T of interest. Along the melting curve of pure pyrope, $\Delta G_{f(P,T)}^0 = 0$, and after rearranging we obtain

$$\Delta H_{f(0.1,T_f)}^0 - T\Delta S_{f(0.1,T_f)}^0 = -\int_{T_f}^{T} \Delta C_P^0 dT + T\int_{T_f}^{T}\left(\frac{\Delta C_P^0}{T}\right)dT$$
$$- \int_{0.1MPa}^{P} \Delta V^0 dP \qquad (6)$$

Following the terminology of Wood and Blundy (1997), the left hand side of Eq. (6) is referred to as the 'apparent 0.1 MPa free energy of fusion', or apparent $\Delta G_{f,0.1}^0$, because it represents the free energy of (metastable) congruent pyrope fusion at $P = 0.1$ MPa, after removal of the heat capacity and volume terms. This removal linearises Eq. (6) with respect to temperature (Wood and Blundy 1997).

The integrals on the right hand side of Eq. (6) can be evaluated by combining published P–T points along the pyrope melting curve with thermochemical data on pyrope crystal and pyrope melt. The melting curve of pyrope has been studied over the pressure range of 3.5 to 25 GPa (Irifune and Ohtani 1986; Zhang and Herzberg 1994; Shen and Lazor 1995). Below 3.5 GPa, pyrope melts incongruently (e.g. Boyd and England 1962) and free energy of melting information cannot be obtained. The studies of Irifune and Ohtani (1986) and Zhang and Herzberg (1994) both report a kink in the melting curve at high pressure ($P > 10$ GPa), which they attribute to pressure-induced coordination changes of Al in pyrope liquid, or to disordering in pyrope crystals. Because we are primarily interested in partial melting of garnet at upper mantle pressures, we only incorporated melting experiments at pressures below 10 GPa into our thermodynamic analysis.

The thermochemical data used for modelling the pyrope melting curve are given in Table 1. Heat capacities for pyrope melt were calculated from values for the constituent oxides (Lange and Carmichael 1990), as were melt volumes (V^0), compressibilities (K), and expansivities (α) (Lange and Carmichael 1990). Several heat capacity equations for pyrope were considered (Berman 1988; Téqui et al. 1991; Robie and Hemingway 1995). The Berman (1988) equation was chosen because it was found to give more stable results at the high temperatures (up to 2,300 K) involved. dK/dP (K') for solid pyrope, and its derivative, were taken from Webb (1989). V^0 and α for pyrope crystals were from Zhang and Herzberg (1994). The Grüneisen parameter was assumed to be 1.5. Finally, solid pyrope bulk modulus and its temperature derivatives are from the compilation of Bass (1995). The pressure integral in Eq. (6) was evaluated using integration by parts of the Birch–Murnaghan equation of state (as in Blundy et al. 1995; Wood and Blundy 1997).

Table 1 Thermodynamic data used in modelling of pyrope melting reaction

Parameter	Unit	Pyrope		Melt	
		Value	Source[a]	Value	Source[a]
V^0	kJ GPa^{-1} mol^{-1}	113.37	1	143.2	5
α^0	K^{-1}	2.43×10^{-5}	1	1.22×10^{-5}	5
K	GPa	175	2	20.9	5
$\partial K/\partial T$	GPa K^{-1}	–0.02	2	–0.0017	b
$\partial^2 K/\partial T^2$	GPa K^{-2}	-1.8×10^{-5}	2	–	–
K'	–	4.5	3	7.0	b
$\partial^2 K/\partial P^2$	GPa^{-1}	–0.028	3	–	–
$C_p{}^c$					
a	kJ mol^{-1} K^{-1}	–0.54805	4	0.6967	5
b	kJ mol^{-1}	–1.22075	4	–	–
c	kJ mol^{-1}	–244,240	4	–	–
d	kJ mol^{-1}	3,255,200	4	–	–

[a]Sources: (1) Zhang and Herzberg (1994); (2) Bass (1995); (3) Webb (1989); (4) Téqui et al. (1991); (5) Lange and Carmichael (1990)
[b]Estimate
[c]$C_p = a + bT^{-0.5} + cT^{-2} + dT^{-3}$ after Berman (1988)

The resulting variation in the apparent 0.1 MPa free energy of fusion with temperature is given in Fig. 2. The slope of the resulting linear trend should equal the real 0.1 MPa entropy of fusion of pyrope, $\Delta S^0_{f(0.1,T_f)}$, while the intercept should give $\Delta H^0_{f(0.1,T_f)}$, the 0.1 MPa enthalpy of fusion. Our regressed values, $\Delta H^0_{f(0.1,T_f)} = 243 \pm 16\,\text{kJ mol}^{-1}$ and $\Delta S^0_{f(0.1,T_f)} = 151 \pm 7\,\text{J mol}^{-1}\,\text{K}^{-1}$, are in excellent agreement with the calorimetric data of Newton et al. (1977) ($\Delta H^0_{f(0.1,T_f)} = 243 \pm 8$ kJ mol^{-1}; $\Delta S^0_{f(0.1,T_f)} = 162 \pm 5$ J mol^{-1} K^{-1}) and the study of Téqui et al. (1991) ($\Delta H^0_{f(0.1,T_f)} = 241.9$, kJ mol^{-1}, $\Delta S^0_{f(0.1,T_f)} = 154.1$ J mol^{-1} K^{-1}).

In natural systems where garnet and melt coexist, the two phases are not pure pyrope, so ΔG^0_f in Eq. (5) does not equal zero, but depends on the activities (a) of the pyrope component ($Mg_3Al_2Si_3O_{12}$) in garnet and melt:

$$\Delta G^0_{f(P,T)} = RT \ln \left(\frac{a_{Py}^{garnet}}{a_{Py}^{melt}} \right) \tag{7}$$

For multi-component garnet–melt equilibria, Eq. (6) has to be adjusted to incorporate the mixing of components in both garnet and melt:

$$\Delta H^0_{f(0.1,T_f)} - T\Delta S^0_{f(0.1,T_f)} = -\int \Delta C^0_P dT + T \int \left(\frac{\Delta C^0_P}{T} \right) dT$$
$$- \int \Delta V^o dP + RT \ln \left(\frac{a_{Py}^{garnet}}{a_{Py}^{melt}} \right) \tag{8}$$

If good activity–composition models can be obtained for $Mg_3Al_2Si_3O_{12}$ in both garnet and melt, $\Delta H^0_{f(0.1,T_f)}$ and $\Delta S^0_{f(0.1,T_f)}$ for pyrope obtained from the compositions of natural garnet–melt pairs [using Eq. (8)] should be comparable to $\Delta H^0_{f(0.1,T_f)}$ and $\Delta S^0_{f(0.1,T_f)}$ derived from the pyrope melting curve using Eq. (6) (Fig. 2). The simplest possible activity model for the activity of $Mg_3Al_2Si_3O_{12}$ in garnet is that it equals the cube of the mole fraction of Mg on the garnet X-site, and that mixing on the X-site is ideal:

$$a_{Mg_3Al_2Si_3O_{12}}^{garnet} = \left(X_{Mg}^{garnet} \right)^3 \tag{9}$$

where $X_{Mg}^{garnet} = Mg/(Mg + Fe^{2+} + Ca + Mn)$. As a first approximation, garnet non-ideality is therefore ignored (but see below). For the melt, an equally simple assumption is made (following Wood and Blundy 1997), namely assuming ideal mixing of $Mg_3Al_2Si_3O_{12}$ with other silicate melt components on a 12 oxygen basis.

$$a_{Mg_3Al_2Si_3O_{12}}^{melt} = \left(X_{Mg}^{melt} \right)^3 \tag{10}$$
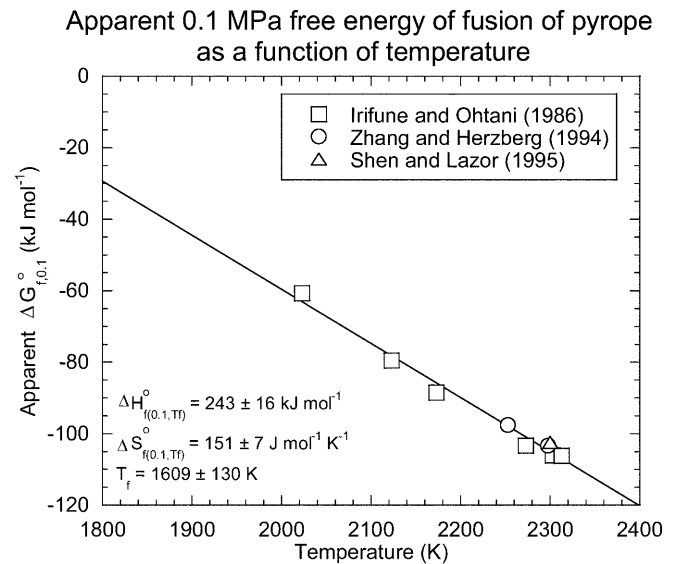
Fig. 2 Regression of pyrope ($Mg_3Al_2Si_3O_{12}$) melting curve data to Eq. (6), using data from Table 1. 0.1 MPa enthalpies and entropies of fusion ($\Delta H^0_{f(0.1,T_f)}$ and $\Delta S^0_{f(0.1,T_f)}$) given by the slope and intercept of the regression line. Metastable 0.1 MPa melting point of pyrope, T_f, given by $\Delta H^0_{f(0.1,T_f)}/\Delta S^0_{f(0.1,T_f)}$

where X_{Mg}^{melt} refers to the number of Mg atoms per 12 oxygens in the melt. Using Eqs. (9) and (10), and assuming that the mean molecular weights of garnets and melts are equal, Eqs. (7) and (8) now become

$$\Delta G_{f(P,T)}^0 = RT \ln \left(\frac{\left(X_{Mg}^{garnet} \right)^3}{\left(X_{Mg}^{melt} \right)^3} \right) = 3RT \ln \left(\frac{X_{Mg}^{garnet}}{X_{Mg}^{melt}} \right) \cong 3RT \ln D_{Mg}$$

(11)

and

$$\Delta H_{f(0.1,T_f)}^0 - T\Delta S_{f(0.1,T_f)}^0 = - \int \Delta C_P^0 dT + T \int \left(\frac{\Delta C_P^0}{T} \right) dT$$
$$- \int \Delta V^o dP + 3RT \ln D_{Mg}$$

(12)

The assumption of equal mean molecular weights of garnet and melt is very reasonable: the variation in mean molecular weight (on a 12 oxygen basis) is between 0 and 2% relative in anhydrous experiments, and between 2 and 8% for hydrous experiments. We have tested our model by plotting the right hand side of Eq. (12) against temperature for a large number ($n = 160$) of garnet–melt pairs taken from the literature. Because P and T are vital input parameters for the model, no natural data were used. Systems containing less than 0.5 wt% of Mg in either garnet or melt were excluded, because of the large errors involved in Mg electron probe analysis. Compositional data were found for 66 garnet–anhydrous melt pairs, and 94 garnet–hydrous melt pairs. The anhydrous data span a T range of 1,703–2,202 K, and a P range of 2.5–7.5 GPa. Temperatures in published hydrous experiments containing garnet are between 1,123 and 1,563 K, with pressures between 1.0 and 3.0 GPa. This data set therefore spans the whole range of P–T conditions relevant to upper mantle melting.

The resulting plot is shown in Fig. 3. The anhydrous data (dots) display a linear trend, comparable to the trend shown in Fig. 2 for the pyrope melting curve. Regression of the anhydrous data leads to $\Delta H_{f(0.1,T_f)}^0 = 288 \pm 20$ kJmol^{-1}, $\Delta S_{f(0.1,T_f)}^0 = 183 \pm 10$ J mol^{-1}K^{-1}, and a hypothetical 0.1 MPa melting point for pyrope of $1,575 \pm 145$ K. $\Delta H_{f(0.1,T_f)}^0$ and $\Delta S_{f(0.1,T_f)}^0$ are therefore slightly higher than values derived from the melting curve, while T_f is the same within error. Although agreement is not perfect, it is remarkable that simple activity–composition relations seem to work so well, and that simple relationships are found between garnet–melt magnesium partitioning data and the pyrope melting curve. Data from hydrous experiments generally fall below the trend seen in the anhydrous data. Although beyond the scope of this paper, we note that Blundy and Wood (1999) have developed a quantitative expression relating the activities of Mg components in silicate melts to melt water content. By taking into account this effect on the activity of pyrope in the melt, the apparent free energies plotted in Fig. 3 for samples with 5–10 wt% water are increased by 15–20 kJ mol^{-1}. This correction would bring most of the hydrous samples directly in line with the trend extrapolated from the anhydrous data.
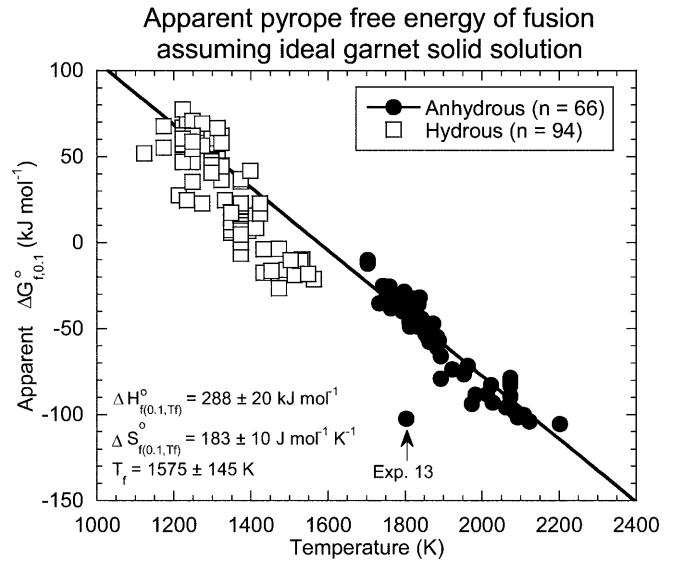
Fig. 3 Variation in apparent 0.1 MPa free energy of fusion of pyrope, $\Delta G_{f,0.1}^0$, with T calculated from garnet–melt Mg partitioning data. *Circles* data from anhydrous experiments, taken from Nicholls and Harris (1980), Takahashi (1986), Trønnes et al. (1992), Hauri et al. (1994), Walter and Presnall (1994), Yasuda et al. (1994), Longhi (1995), Gudfinnsson and Presnall (1996), Herzberg and Zhang (1997), Withers (1997), Johnson (1998), Putirka (1998), Walter (1998), Salters and Longhi (1999), Van Westrenen et al. (1999a, 2000b). *Squares* data from hydrous experiments, taken from Nicholls and Harris (1980), Sen and Dunn (1994), Wolf and Wyllie (1994), Patiño Douce and Beard (1995), Rapp (1995), Rapp and Watson (1995), Barth et al. (1997), Withers (1997), Gaetani and Grove (1998), Rapp et al. (1999), Green et al. (2000). *Line* is a linear fit to anhydrous data alone. Note the anomalous position of anhydrous experiment 13 from Van Westrenen et al. (1999a), and the apparent temperature offset between anhydrous and hydrous experiments at $\Delta G_{f,0.1}^0$ of ± -20 kJ mol^{-1}

The fact that virtually all anhydrous experimental data fall on one straight line suggests that the role of garnet non-ideality on Mg partitioning is small compared to the effects of temperature and pressure. The one point (experiment 13 from Van Westrenen et al. 1999a, see Fig. 1a) that deviates significantly from near-ideal behaviour is for an extremely calcic garnet of composition Py$_9$Gr$_{91}$. In this case, given the observed non-ideality in Ca–Mg garnets (e.g. Newton et al. 1977; Berman 1988, 1990; Wood 1988; Ganguly et al. 1993; Berman and Aranovich 1996; Bosenick and Geiger 1997; Mukhopadhyay et al. 1997), non-ideality is almost certainly significant. To increase the general applicability of our model, in the next section we derive a quantitative model for this non-ideality, using as a basis the garnet–melt partitioning experiments of Van Westrenen et al. (1999a, Fig. 1).

Garnet non-ideality and garnet–melt partitioning data

Because of the apparent success of using simple activity–composition relations, we decided to treat the partitioning of trivalent trace elements in a similar fashion

to our treatment of magnesium partitioning outlined above. Few data are available on the substitution mechanism of REE into natural garnet. Suggestions include coupled substitutions with a $1+$ cation on the X-site (e.g. Enami et al. 1995), with Mg/Fe/Ca/Mn on the Y-site (majorite substitution) or with Al on the Z-site (YAG substitution). Van Westrenen et al. (2000a), in their computer simulation of REE incorporation into silicate garnets, predicted that coupling with Li on the X-site would be the most energy-efficient substitution at low temperatures. Unfortunately, this charge-balancing mechanism cannot be tested reliably in the context of activity–composition relations. The garnet–melt partitioning database is small as it is, and combined data for Li, Na and REE partitioning in the same experiment are virtually non-existent. One of the reasons for this is that Na is normally measured by electron microprobe, and Na levels in garnets are usually close to, or below, detection limit. Li partitioning data only exist for a few experiments at 3.0 GPa over a limited temperature range (Withers 1997; Van Westrenen et al. 1999a).

Alternatively, the stability of REE–aluminium garnets such as yttrium aluminium garnet (YAG, $Y_3Al_5O_{12}$) suggests that charge-balancing REE in the garnet X-site can be effectively achieved by substituting Al for Si on the garnet Z-site. We therefore decided to study a melting reaction, similar to the one for pyrope [Eq. (4)], for a simple REE–pyrope component with a YAG-type charge-balancing mechanism, $J^{3+}Mg_2Al_2^{VI}$-$(Al^{IV}Si_2)O_{12}$:

$$J^{3+}Mg_2Al_3Si_2O_{12}(garnet) = J^{3+}Mg_2Al_3Si_2O_{12}(melt) \qquad (13)$$

J^{3+} is a fictive REE with radius $r_0(3+)$. Again we assume that solid and liquid phases obey ideal activity–composition relations similar to those used for pyrope above, jadeite (Blundy et al. 1995) and diopside (Wood and Blundy 1997). Assuming complete ordering on the garnet Y- and Z-sites, and a melt model analogous to the case of $Mg_3Al_2Si_3O_{12}$, we obtain

$$a_{JMg_2Al_3Si_2O_{12}}^{garnet} = \frac{27}{4}X_J^{garnet}\left(X_{Mg}^{garnet}\right)^2 \qquad (14)$$

where X_J^{garnet} is the mole fraction of J on the X-site, and

$$a_{JMg_2Al_3Si_2O_{12}}^{melt} = \frac{27}{4}X_J^{melt}\left(X_{Mg}^{melt}\right)^2 \qquad (15)$$

where X_J^{melt} is the number of atoms of J per 12 oxygens. The factor 27/4 ensures that the activity of these components in pure systems is equal to unity. Making these assumptions, and again noting that molecular weights of garnet and melt can be assumed identical, the reciprocal of the equilibrium constant for Eq. (13) (K_{13}) is given by:

$$\frac{1}{K_{13}} = \frac{a_{JMg_2Al_3Si_2O_{12}}^{garnet}}{a_{JMg_2Al_3Si_2O_{12}}^{melt}} = D_0(3+)D_{Mg}^2 \qquad (16)$$

At a given P and T, the equilibrium constant K should be constant. In Fig. 4, values of reciprocal K_{13} calculated using Eq. (16) are shown as a function of garnet composition (squares) for the isobaric, near-isothermal

partitioning data of Van Westrenen et al. (1999a). Clearly $1/K_{13}$ is not constant in this case, which means Eq. (16) does not give a complete description of the thermodynamics of Eq. (13). We note that the most calcic sample in Fig. 4 (experiment 13 of Van Westrenen et al. 1999a) again deviates significantly from other garnet–melt pairs formed at the same temperature, when assuming ideal mixing. The most obvious explanation for these discrepancies is that they result from garnet non-ideality.

Because of their importance in geothermobarometry, non-ideal behaviour and activity–composition relations in garnets have received a great deal of attention (e.g. Newton et al. 1977; Berman 1988, 1990; Wood 1988; Ganguly et al. 1993; Berman and Aranovich 1996; Bosenick and Geiger 1997; Mukhopadhyay et al. 1997). An important conclusion from all of these studies is that there is significant non-ideality along the pyrope–grossular join, while the effects along the other joins are much smaller. This non-ideality results in the activity of pyrope in garnet not being equal to the cube of its mole fraction. X_{Mg} in Eq. (14) should be multiplied by an appropriate activity coefficient, γ_{Mg}^{garnet}, and the equilibrium constant [Eq. (16)] should be adjusted accordingly:

$$\frac{1}{K_{17}} = \frac{a_{JMg_2Al_3Si_2O_{12}}^{garnet}}{a_{JMg_2Al_3Si_2O_{12}}^{melt}} = D_0(3+)D_{Mg}^2\gamma_{Mg,garnet}^2 \qquad (17)$$

Effect of garnet non-ideality on apparent equilibrium constant at P = 3 GPa, T = 1545 ^{o}C
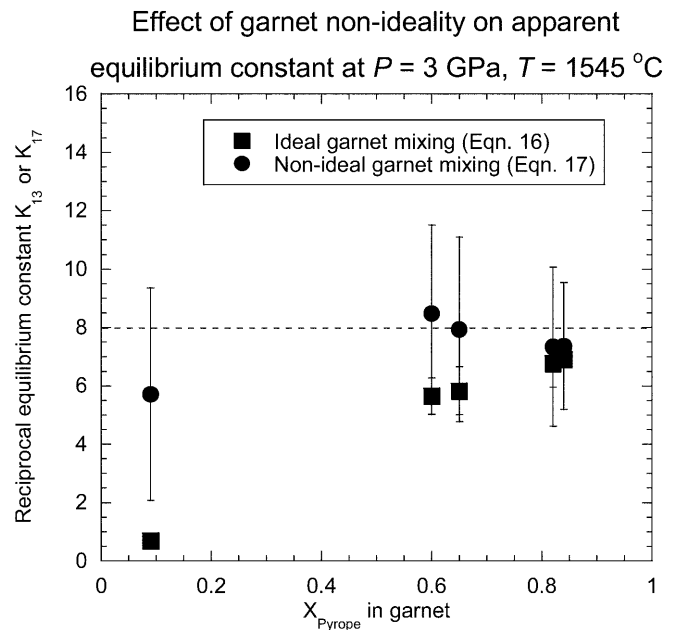
Fig. 4 The effect of incorporating garnet non-ideality into activity–composition relations for the hypothetical garnet $J^{3+}Mg_2Al_3Si_2O_{12}$, with J a fictive REE with optimum radius $r_0(3+)$ (see text for explanation). *Squares* are calculated values of K_{13} [using Eq. (16)], assuming ideal garnet solid solutions, for garnet–melt partitioning experiments in CMAS (Van Westrenen et al. 1999a). *Circles* are calculated values of K_{17} [Eq. (17)] for the same experiments, using Eq. (17), assuming a simple symmetrical excess enthalpy of mixing

When $X_{Mg}^{garnet} = 1$ (i.e. in pure pyrope), γ_{Mg}^{garnet} must equal unity. We therefore derived a value for $1/K_{17}$ in pure pyrope, applicable to the P–T conditions of the experiments by Van Westrenen et al. (1999a; $P = 3$ GPa, $T = 1,545 \pm 15$ °C), by linear extrapolation of the data shown in Fig. 4. The extrapolated value of $1/K_{17}$ at $X_{Mg}^{garnet} = 1$ is 8.0 ± 0.4. K_{17} is equal for all experiments along the Py–Gr join performed under these P–T conditions.

We used a subregular Margules model to derive the excess enthalpy of mixing (H^{XS}) required to adjust all reciprocal K_{17} values calculated using Eq. (16) to a value of $1/K_{17}$ of 8.0. In the Margules model of excess thermodynamic properties the excess enthalpy of pyrope–grossular garnets depends on the mole fractions of Ca and Mg, and the interaction coefficients W_{CaMg} and W_{MgCa}. Using the generalised formula of Helffrich and Wood (1989), we obtain:

$$H^{XS} = W_{CaMg}X_{Ca}X_{Mg}^2 + W_{MgCa}X_{Ca}^2X_{Mg} \tag{18}$$

If we assume a symmetrical model, the Margules parameters $W_{CaMg} = W_{MgCa} = W^H$, and Eq. (18) is simplified to:

$$H^{XS} = W^H X_{Ca}X_{Mg}^2 + W^H X_{Ca}^2 X_{Mg} = W^H X_{Ca}(1 - X_{Ca}) \tag{19}$$

Again following Helffrich and Wood (1989), a general expression can be derived for γ_{Mg}^{garnet} in binary Py–Gr mixtures:

$$RT\ln\left(\gamma_{Mg}^{garnet}\right) = \frac{1}{2}W_{MgCa}X_{Ca}\big[1 - X_{Mg} + X_{Ca}$$
$$+ 2X_{Mg}\left(X_{Mg} - X_{Ca} - 1\right)\big] + \frac{1}{2}W_{CaMg}X_{Ca}$$
$$\times \big[1 - X_{Mg} - X_{Ca} - 2X_{Mg}\left(X_{Mg} - X_{Ca} - 1\right)\big] \tag{20}$$

When the excess enthalpy is assumed symmetrical (i.e. $W_{CaMg} = W_{MgCa} = W^H$), this simplifies to

$$RT\ln\left(\gamma_{Mg}^{garnet}\right) = \frac{1}{2}W^H X_{Ca} \cdot 2\left[1 - X_{Mg}\right] = W^H X_{Ca}^2 \tag{21}$$

Combining Eqs. (16) and (17), and assuming our predicted $1/K_{17}$ of 8.0 for pure Py, we obtain

$$RT\ln\left(\gamma_{Mg}^{garnet}\right) = RT\ln\left(\sqrt{\frac{K_{13}}{K_{17}}}\right) = \frac{1}{2}RT\ln\left(\frac{8.0}{D_0(3+)D_{Mg}^2}\right) \tag{22}$$

From Eqs. (21) and (22), we can see that a value for W^H (assuming the simplest case of symmetrical solution) can be obtained from a plot of the right hand side of Eq. (22) against garnet grossular content (X_{Ca}). This is done in Fig. 5a. A weighted parabolic fit to the data gives a best-fit value of 19 ± 3 kJ mol^{-1} (on a one cation basis) for W^H. When this factor is incorporated into Eq. (21) to calculate appropriate activity coefficients for Mg, the resulting values of K_{17} calculated using Eq. (17) are all within error of 8.0 (circles in Fig. 4). This means that Eq. (17) gives a good description of the thermodynamics of the reaction Eq. (13). In Fig. 5b, the excess enthalpy along the Py–Gr join that we predict by incorporating our estimate of W^H into Eq. (19) is compared with literature data. Firstly, our predicted H^{XS} is in reasonable
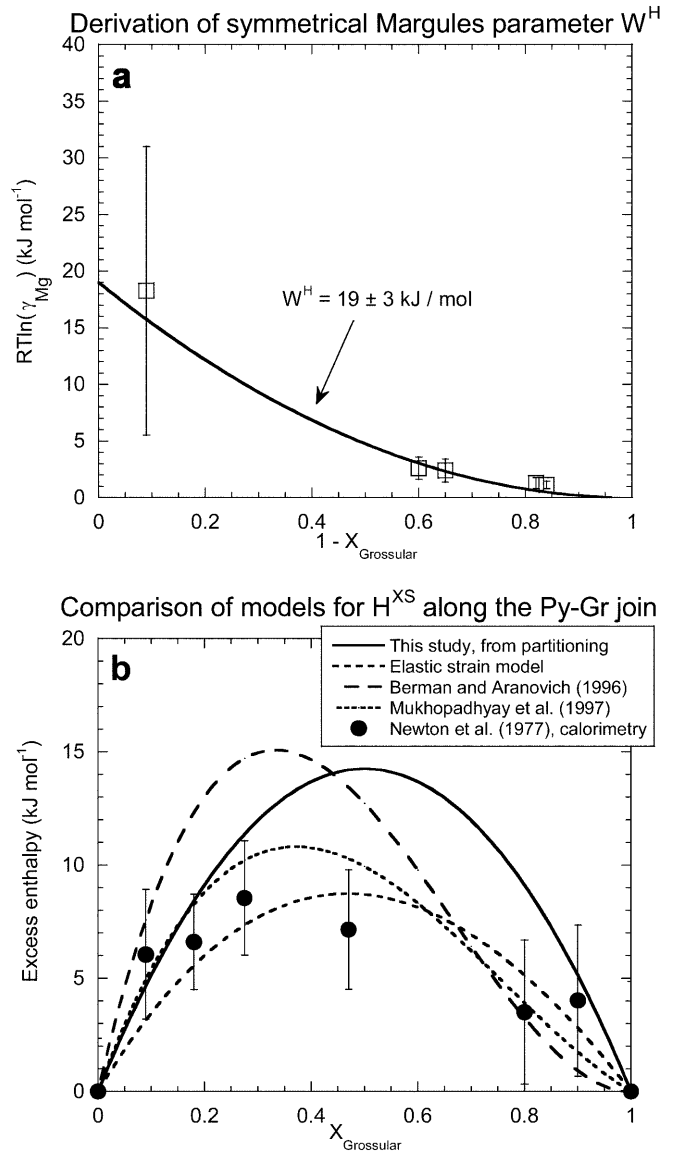
Fig. 5 a Derivation of symmetrical Margules parameter (W^H) for the Py–Gr join from experimental garnet–melt partitioning data (Van Westrenen et al. 1999a). b Comparison of excess enthalpy along the Py–Gr join derived from partitioning data (Fig. 3) with calorimetric data, elastic strain model and thermodynamic mixing models

agreement with calorimetric measurements of excess enthalpies by Newton et al. (1977). Most garnet mixing models assume an asymmetrical excess enthalpy on the basis of the higher average calorimetric excesses on the pyrope-rich part of the join, but the errors on calorimetric values are relatively large and a symmetrical model seems equally justifiable.

Our excess enthalpy, which it should be stressed was derived from knowledge of garnet–melt trace element partitioning under isobaric, isothermal conditions, gives as good an agreement with the calorimetric values as the Berman and Aranovich (1996) model which is based on a weighted regression analysis of available volumetric, calorimetric and phase equilibrium data. If we use the lattice

strain model of Brice (1975) to calculate excess enthalpies along the Py–Gr join we obtain slight asymmetry, with $W_{CaMg} = 13.1$ kJ mol^{-1} and $W_{MgCa} = 10.1$ kJ mol^{-1} (on a one cation basis) which is in reasonable agreement with our symmetrical value of 19 ± 3 kJ mol^{-1}. We conclude that our model for garnet non-ideality is in reasonable agreement with our current knowledge of garnet thermodynamics, and is able to explain the variation in K along the Py–Gr join observed in Fig. 4.

For the large majority of garnets from experimental garnet–melt pairs found in the literature, the activity of Mg is very close to its mole fraction: γ_{Mg}^{garnet} is within 10% of unity. The three exceptions are found in the relatively Ca-rich samples from the study of Van Westrenen et al. (1999a) discussed above (Fig. 4). In the next section, we briefly discuss the effect of incorporating our non-ideality model into our analysis of the partitioning of Mg between garnet and melt, before providing a predictive model for $D_0(3+)$ as a function of P and T.

A model for D_{Mg}

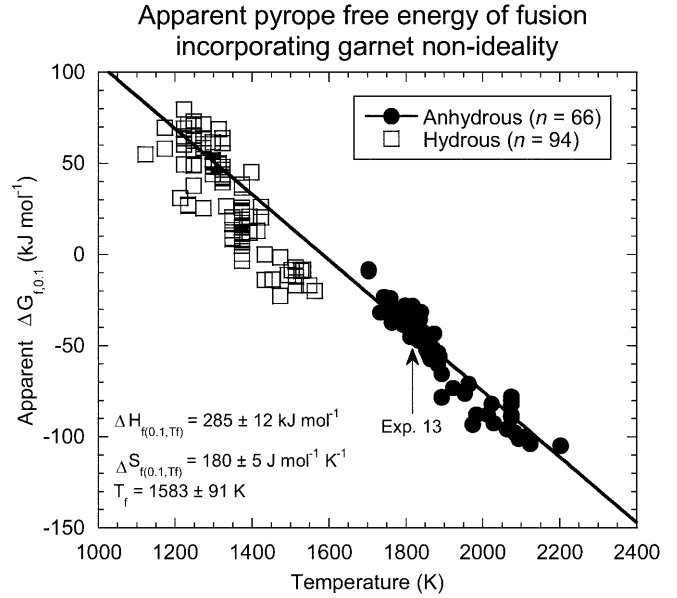Incorporating our model for non-ideality into our model of Mg distribution [Eq. (12)], we derive

$$\Delta H_{f(0.1,T_f)}^0 - T \Delta S_{f(0.1,T_f)}^0 = -\int \Delta C_P^0 dT + T \int \left(\frac{\Delta C_P^0}{T}\right) dT$$
$$- \int \Delta V^o dP + 3RT \ln\left(\gamma_{Mg}^{garnet} D_{Mg}\right) \quad (23)$$

Figure 6 shows the resulting effect on the calculated apparent 0.1 MPa free energy of fusion data previously shown in Fig. 3. The anomaly for experiment 13 from Van Westrenen et al. (1999a) has disappeared completely. Using anhydrous data only, fitted values of $\Delta H_{f(0.1,T_f)}^0$ (285 ± 12 kJ mol^{-1}) and $\Delta S_{f(0.1,T_f)}^0$ (180 ± 5 J mol^{-1} K^{-1}), and resulting prediction of the fictive melting point of pyrope at atmospheric pressure ($T_f = 1,583 \pm 91$ K) are close to the values derived previously assuming ideal garnet solid solution, and within 2 standard deviations of the calorimetric data. The offset between trends in anhydrous versus hydrous data has remained the same after incorporation of garnet non-ideality, and the explanation of Blundy and Wood (1999) for this offset remains valid.

The agreement of our very simple model with the melting curve (or calorimetric) data is as good as the recent study of garnet + liquid equilibrium of Putirka (1998). He used linear least squares analysis of experimental data obtained at pressures up to 27 GPa, and derived best-fit values of 194 ± 50 kJ mol^{-1} for $\Delta H_{f(0.1,T_f)}^0$ and 107 ± 28 J mol^{-1} K^{-1} for $\Delta S_{f(0.1,T_f)}^0$.

We can use Eq. (23) to predict variations in D_{Mg} as a function of P, T and garnet composition. Rearranging Eq. (23), we obtain:

$$D_{Mg} = \frac{\exp\left(\frac{285000 - 180 \cdot T + \left(\Delta C_p, \Delta V^o \text{ terms}\right)}{3RT}\right)}{\exp\left(\frac{19000 \cdot X_{Ca}^2}{RT}\right)} \quad (24)$$

Apparent pyrope free energy of fusion incorporating garnet non-ideality

Fig. 6 Variation in apparent 0.1 MPa free energy of fusion of pyrope, $\Delta G_{f,0.1}^0$, calculated from garnet–melt Mg partitioning data and incorporating a measure of garnet non-ideality [Eq. (21)]. *Circles* data from anhydrous experiments. *Squares* data from hydrous experiments. Data sources as in the caption of Fig. 3. *Line* is a linear fit to anhydrous data alone. Note that the position of anhydrous experiment 13 from Van Westrenen et al. (1999a) is no longer anomalous, and that the apparent temperature offset between anhydrous and hydrous experiments remains identical to Fig. 3

with T in K, and $R = 8.314$ J mol^{-1} K^{-1}. The ΔC_p, ΔV^0 correction term is derived from thermodynamic data on pure pyrope, and the expression for γ_{Mg}^{garnet} from Eq. (21). The propagated uncertainty in Eq. (24) is 16% (1σ). In Fig. 7, predicted D_{Mg} are compared with measurements.

Keeping in mind the simplicity of our model, the resulting agreement between predicted and measured values is reasonable. We conclude that Eq. (24) can be used to model variations in Mg partitioning between garnet and anhydrous silicate melt over the experimental P–T range of available garnet–melt equilibria, i.e. between temperatures of 1,703 and 2,202 K, and pressures of 2.5 and 7.5 GPa. Our treatment shows that despite their structural complexity, silicate melts can be modelled effectively assuming simple thermodynamic behaviour over the compositional range relevant to partial melting in the mantle. This confirms earlier observations (e.g. Burnham 1981; Blundy et al. 1995; Wood and Blundy 1997).

Equation (24) can also be used, in conjunction with the lattice strain model of Blundy and Wood (1994), to predict garnet–melt partition coefficients for other divalent elements entering the garnet X-site, such as Ca, Sr, and Cd. For example, D_{Sr} can be predicted using

$$D_{Sr} = D_{Mg} \exp\left(\frac{-4\pi E_X(2+)N_A}{RT}\left[\frac{r_0(2+)}{2}\left(r_{Mg}^2 - r_{Sr}^2\right) + \frac{1}{3}\left(r_{Sr}^3 - r_{Mg}^3\right)\right]\right)$$
$$(25)$$

Available data indicate that $r_0(2+)$ for the garnet X-site is consistently 0.04 ± 0.01 Å larger than $r_0(3+)$ (e.g. Van

Comparison between measured and predicted Mg garnet-melt partition coefficients
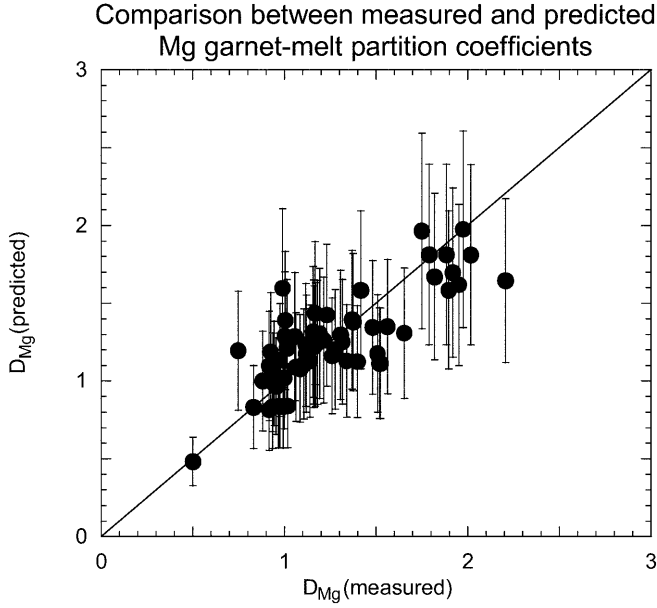
Fig. 7 Comparison between D_{Mg} measured experimentally and D_{Mg} predicted using Eq. (24) for all anhydrous data ($n = 66$). *Error bars* 2σ propagated error in predicted values. *1:1 line* shown for reference

Westrenen et al. 2000a). The parameter $E_X(2+)$ is poorly constrained. Our best (empirical) estimate assumes $E_X(2+) = 2/3 \, E_X(3+)$ (Wood and Blundy 1997), so that $E_X(2+)$ can be approximated via Eq. (3) (using $r_0(2+) = r_0(3+) + 0.04$ Å).

A thermodynamic model for $D_0(3+)$ and predictions of $D_{REE/Y/Sc}$

Having demonstrated the success of our approach in modelling Mg partitioning between garnet and melt, we take an analogous approach to modelling $D_0(3+)$ for the rare earth elements as a function of P and T. Instead of melting pure pyrope, we now look at the melting of the hypothetical rare earth garnet $J^{3+}Mg_2Al_3Si_2O_{12}$, introduced in the previous section, where J^{3+} has ideal radius $r_0(3+)$. Analogous to Eq. (8), we have

$$\Delta H_{f(0.1,T_f)}^0 - T\Delta S_{f(0.1,T_f)}^0 = -\int \Delta C_P^0 dT + T \int \left(\frac{\Delta C_P^0}{T}\right) dT$$
$$- \int \Delta V^o dP + RT \ln\left(\frac{a_{JMg_2Al_3Si_2O_{12}}^{garnet}}{a_{JMg_2Al_3Si_2O_{12}}^{melt}}\right) \quad (26)$$

In this case, the enthalpy, entropy, volume and heat capacity terms all refer to properties of solid and molten $J^{3+}Mg_2Al_3Si_2O_{12}$. None of these data are available for this component, and some simplifying assumptions need to be made. Although ΔC_P^0 terms are unknown, it has been shown previously that they can be assumed zero over wide temperature ranges (Wood and Fraser 1976; Wood and Blundy 1997). Furthermore, in the pressure range relevant to our model the volume of fusion of

$J^{3+}Mg_2Al_3Si_2O_{12}$ can be assumed to be a linear function of pressure. Making these assumptions, and using the simple activity–composition relations developed in Eqs. (14) and (15) we obtain:

$$\Delta H_{f(0.1,T_f)}^0 - T\Delta S_{f(0.1,T_f)}^0 + P\Delta V + \frac{1}{2}\left(\frac{\partial \Delta V}{\partial P}\right)P^2$$
$$= RT \ln\left(\left(\gamma_{Mg}^{garnet} D_{Mg}\right)^2 D_0(3+)\right) \quad (27)$$

From Eq. (27), it can be seen that $\Delta S_{f(P,T_f)}^0$ may be estimated by analysing a set of experiments performed at constant pressure over a wide range of temperatures. In this case, the pressure terms in Eq. (27) are constant, and $\Delta S_{f(P,T_f)}^0$ is obtainable from the slope of a plot of apparent free energy of fusion versus temperature. The anhydrous garnet–melt partitioning database is dominated by experiments performed at 3 GPa (Withers 1997; Johnson 1998; Van Westrenen et al. 1999a, 2000b). After fitting the rare earth element partitioning data to Eq. (1) to obtain $D_0(3+)$, calculated free energies of fusion at 3 GPa are plotted against temperature in Fig. 8. The slope of this line gives a value for $\Delta S_{f(3GPa,T_f)}^0$ at 3 GPa for $J^{3+}Mg_2Al_3Si_2O_{12}$ of 226 ± 23 J mol^{-1} K^{-1}. This is significantly higher than the calorimetric measurements for pyrope (151 ± 7 J mol^{-1} K^{-1}) and the value used for pyrope in our model for D_{Mg} (180 ± 5 J mol^{-1} K^{-1}), but within error of an interpolation between those values and the recently published calorimetric measurement for YAG ($Y_3Al_5O_{12}$), 230 J mol^{-1} K^{-1} (Lin et al. 1999). It therefore appears that replacement of Mg by

3 GPa entropy of fusion for JMg$_2$Al$_3$Si$_2$O$_{12}$ derived from partitioning data
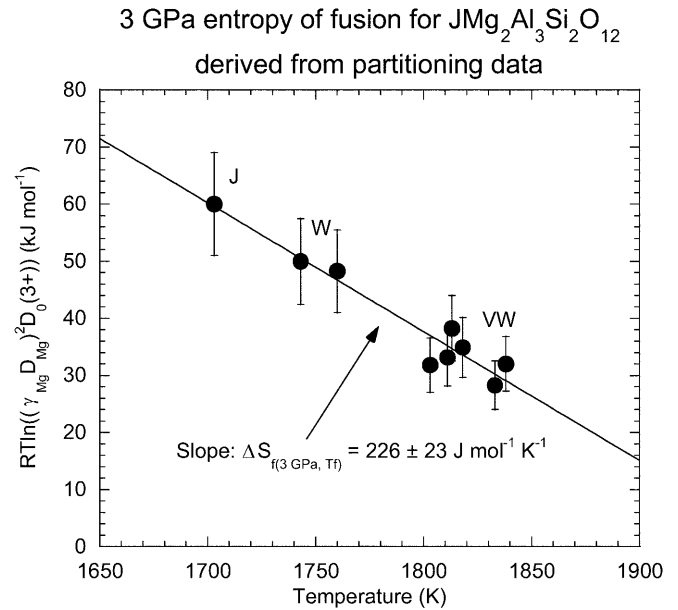
Fig. 8 Derivation of the apparent 3 GPa entropy of fusion for $J^{3+}Mg_2Al_3Si_2O_{12}$. Only data from anhydrous experiments at $P = 3$ GPa are shown. Data sources: *W* Withers (1997), *J* Johnson (1998), *VW* Van Westrenen et al. (1999a, 2000b). *Line* is linear fit through data, with the slope giving $\Delta S_{f(3GPa,T_f)}^0 = 226 \pm 23$ Jmol^{-1}K^{-1}. *Error bars* are 1σ

trivalent cations, charge-balanced by replacing Si by Al, increases the entropy of fusion of the resulting component.

The effect of pressure on $\Delta S^0_{f(P,T_f)}$ is small: over the pressure range from 0.1 MPa to 3 GPa, it is on the order of 1 J mol^{-1} K^{-1} ($\frac{\partial S}{\partial P} = -\alpha V^0$ using data from Table 1) for garnet. This is within the error resulting from our fitting method (23 J mol^{-1} K^{-1}, Fig. 8). We therefore applied our value of $\Delta S^0_{f(3GPa,T_f)}$ to compensate for the temperature effect on all garnet–melt partitioning data irrespective of pressure. This allows us to make an estimate of the volume and enthalpy of fusion of $J^{3+}Mg_2Al_3Si_2O_{12}$. After rearranging, we obtain:

$$RT \ln\left(\left(\gamma^{garnet}_{Mg}D_{Mg}\right)^2 D_0(3+)\right) + 226(23)T$$
$$= \Delta H^0_{f(0.1,T_f)} + P\Delta V + \frac{1}{2}\left(\frac{\partial \Delta V}{\partial P}\right)P^2 \quad (28)$$

By plotting the left hand side of Eq. (28) against pressure (Fig. 9), information is obtained about $\Delta H^0_{f(0.1,T_f)}$ and $\Delta V^0_{f(0.1,T_f)}$. Although the data set is small, the pressure dependence appears to be linear, therefore the pressure derivative of the volume change ($\frac{\partial \Delta V}{\partial P}$) of equation (13) is negligible. From the slope and intercept of the best-fit line in Fig. 9 we derive $\Delta H^0_{f(0.1,T_f)} = 418 \pm 12$ kJ mol^{-1}, and $\Delta V^0_{f(0.1,T_f)} = 10.4 \pm 1.0$ cm3 mol^{-1}. Like $\Delta S^0_{f(0.1,T_f)}$, $\Delta H^0_{f(0.1,T_f)}$ is significantly larger than the value for pyrope. The recent calorimetric data on YAG (Lin et al.
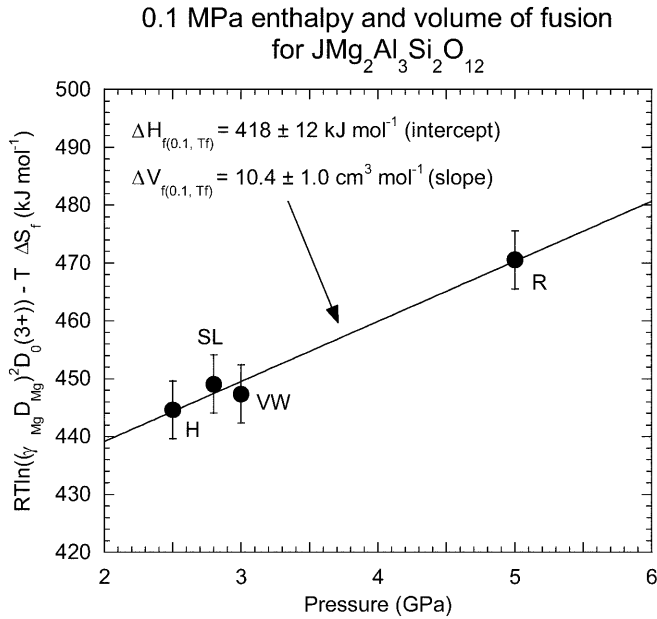
1999) show that YAG has an estimated $\Delta H^0_{f(0.1,T_f)}$ of 516 kJ mol^{-1}. Our derived value of 418 ± 12 kJ mol^{-1} is therefore in line with the progression from pyrope to YAG. We also note that our estimated melting point of $J^{3+}Mg_2Al_3Si_2O_{12}$, $T_f = 1,850 \pm 140$ K, is in between the known values for pyrope ($1,570 \pm 30$ K) and YAG ($1,970 \pm 30$ K, Fratello and Brandle 1993). $\Delta V^0_{f(0.1,T_f)}$ for this rare earth garnet is smaller than the value for pyrope, a trend identical to the one observed for clinopyroxene (Wood and Blundy 1997). There are no $\Delta V^0_{f(0.1,T_f)}$ data for YAG with which to compare.

In conclusion, we believe that these derived values make thermodynamic sense. In Fig. 10, a plot analogous to Fig. 6 is shown for all available anhydrous garnet–melt partitioning literature, plus a subset of hydrous experiments. Again, the hydrous data fall significantly below the predicted trend using anhydrous data only.
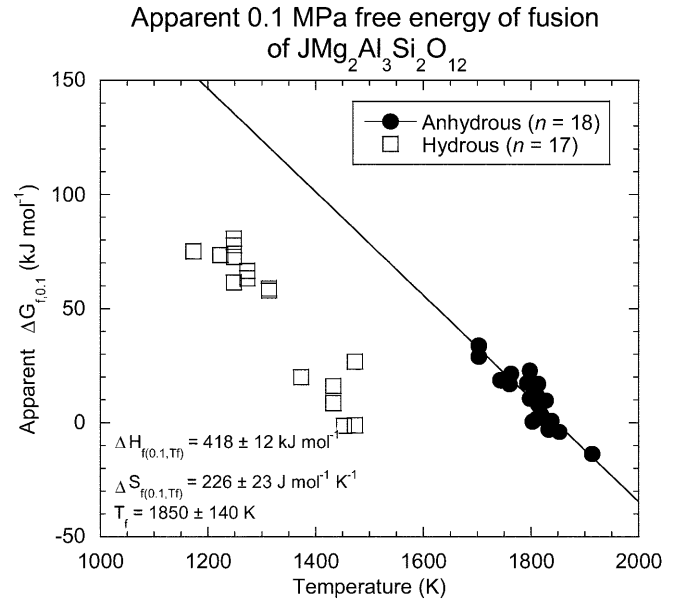
By rearranging Eq. (28) and incorporating the derived values, we arrive at:

$$D_0(3+) = \frac{\exp\left(\frac{418000 + 10400 \cdot P - 226 \cdot T}{RT}\right)}{\left(\gamma^{garnet}_{Mg}D_{Mg}\right)^2} \quad (29)$$

with P in GPa, T in K, and $R = 8.314$ J mol^{-1} K^{-1}. At any given P, T and composition $D_0(3+)$ can now be calculated. The propagated error in $D_0(3+)$ is on the order of 15% (1σ). If melt composition is not known, D_{Mg} can be predicted using Eq. (24), provided crystal composition is known. Garnet composition is necessary

0.1 MPa enthalpy and volume of fusion for $JMg_2Al_3Si_2O_{12}$

$\Delta H_{f(0.1, Tf)} = 418 \pm 12$ kJ mol^{-1} (intercept)

$\Delta V_{f(0.1, Tf)} = 10.4 \pm 1.0$ cm^3 mol^{-1} (slope)

Fig. 9 Derivation of the enthalpy and volume of fusion for fictive rare earth garnet $J^{3+}Mg_2Al_3Si_2O_{12}$. Only averaged values of temperature-corrected energies for data from anhydrous experiments were used. *Error bars* are 1σ. *Line* is linear fit through data, giving $\Delta H^0_{f(0.1,T_f)} = 418 \pm 12$ kJmol^{-1} (intercept) and $\Delta V^0_{f(0.1,T_f)} = 10.4 \pm 1.0$ cm3mol^{-1} (slope). Data sources: *H* Hauri et al. (1994), *R* Rocholl et al. (1996), *SL* Salters and Longhi (1999), *VW* Van Westrenen et al. (1999a, 2000b)

Apparent 0.1 MPa free energy of fusion of $JMg_2Al_3Si_2O_{12}$

Anhydrous ($n = 18$)
Hydrous ($n = 17$)

$\Delta H_{f(0.1,Tf)} = 418 \pm 12$ kJ mol^{-1}

$\Delta S_{f(0.1,Tf)} = 226 \pm 23$ J mol^{-1} K^{-1}

$T_f = 1850 \pm 140$ K

Fig. 10 Variation in apparent 0.1 MPa free energy of fusion, $\Delta G^0_{f,0.1}$, of $JMg_2Al_3Si_2O_{12}$ calculated from garnet–melt REE partitioning data and incorporating a measure of garnet nonideality [Eq. (21)]. *Circles* data from anhydrous experiments, taken from Hauri et al. (1994), Rocholl et al. (1996), Withers (1997), Johnson (1998), Salters and Longhi (1999), Van Westrenen et al. (1999a, 2000b). *Squares* data from hydrous experiments, taken from Barth et al. (1997), Withers (1997), Green et al. (2000). *Line* is a linear fit to anhydrous data alone

to calculate γ_{Mg}^{garnet}, but for most garnets thought to be present in the mantle γ_{Mg}^{garnet} is within 10% of unity. A combination of Eqs. (2), (3) and (29) can be used to predict garnet–anhydrous melt partition coefficients for the REE, Y and Sc in anhydrous systems as a function of P, T and X in the pressure and temperature range relevant to mantle melting. Table 2 gives a summary of our predictive equations, and a spreadsheet that performs all calculations is available. (A Microsoft Excel spreadsheet that performs these calculations can be obtained from the authors or downloaded at http://www.gl.ciw.edu/~van_westrenen/links.html.) For Sc,

predicted D values are *minimum* values, as our model takes account of Sc entering the garnet X-site only; particularly in Ca-rich garnets, significant additional Sc will enter the Y-site as well and real D values will exceed predicted D values.

In Fig. 11a–d we compare predictions using Eqs. (2), (3) and (29) (curves in Fig. 11) with measured data (open symbols) for four experiments covering a wide range of P (2.5–5 GPa) and T (1,703–1,858 K) conditions. The agreement between prediction and observation is good, with deviations varying from 5 to 50% for all elements except the LREE Ce and La. This is true both for ex-

Table 2 Summary of equations that predict garnet–melt trace element partition coefficients as a function of P, T and X

$r_0(3+)$ [Å]	=	$0.930 \cdot X_{Py} + 0.993 \cdot X_{Gr} + 0.916 \cdot X_{Alm} + 0.946 \cdot X_{Spes} + 1.05 \cdot (X_{And} + X_{Uv})$ $-0.005 \cdot (P \text{ [GPa]} - 3.0)$
$E_X(3+)$ [GPa]	=	$3.5 \cdot 10^{12} \cdot (1.38 + r_0(3+)[\text{Å}])^{-26.7}$
$D_0(3+)$	=	$\dfrac{\exp\left(\dfrac{418000 + 10400 \cdot P[\text{GPa}] - 226 \cdot T[\text{K}]}{8.314 \cdot T[\text{K}]}\right)}{\left(\gamma_{Mg}^{garnet} D_{Mg}\right)^2}$
γ_{Mg}^{garnet}	=	$\exp\left(\dfrac{19000 \cdot X_{Ca}^2}{8.314 \cdot T[\text{K}]}\right)$

Fig. 11 Comparison between measured (*symbols*) and predicted (*curves*) values of $D^{Grt/Melt}$ for four experimental partitioning data sets taken from **a** Rocholl et al. (1996), **b** Johnson (1998), **c** Salters and Longhi (1999) and **d** Hauri et al. (1994). Note poor agreement for Yb and Lu in **d**. Predicted values of r_0, D_0 and E_X are from Eqs. (2), (3) and (29) (see Table 2)
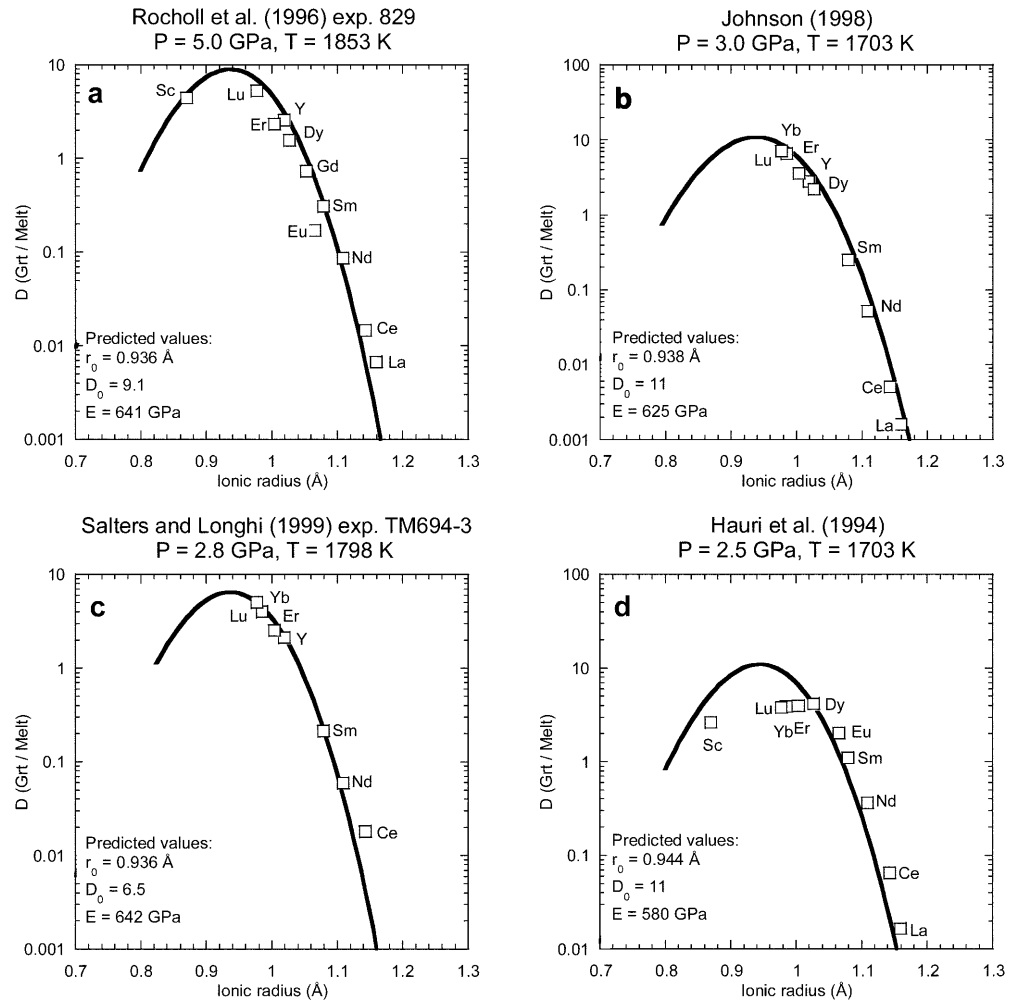
periments that were used in the development of our model (Fig. 11a, b) and for experiments that were not used in our calibration (Fig. 11c).

Our model can also be used to detect anomalies in garnet–melt partitioning data, as shown in Fig. 11d for the experimental results of Hauri et al. (1994). In this case, our model predicts garnet–melt D values for the HREE that are a factor of two to three higher than measured. The flat HREE pattern shown in Fig. 11d seems to be inconsistent with our model. This confirms our earlier view (Van Westrenen et al. 2000b) that the flat pattern of Hauri et al. (1994) is anomalous. This may be a result of the garnets in this study being significantly zoned (Hauri, personal communication).

Figure 12 shows a comparison between predicted and measured values for all garnet–anhydrous melt partition coefficients published to date (a total of 157 data points from 18 different experiments). Agreement for D values between 0.1 and 10, the range generally spanned by trace elements ranging from Nd to Lu, plus Y and Sc, is very good. At lower $D^{\mathrm{Grt/Melt}}$ values (for trace elements La and Ce in particular), measured D values of several studies exceed predicted values by up to an order of magnitude. This is *not* an artefact of the model. As discussed in our earlier study (Van Westrenen et al. 2000b), for very incompatible elements even small amounts of glass contamination during trace element analysis of garnet crystals can lead to large shifts in measured D values. This is illustrated by the dashed lines in Fig. 12, which show the change in measured $D^{\mathrm{Grt/Melt}}$ by 0.2 and 1 wt% glass addition during garnet analysis. Effects of contamination become progressively larger with decreasing D values, consistent with the increase in scatter with decreasing $D^{\mathrm{Grt/Melt}}$ shown in Fig. 12. It is very difficult to prove that such small amounts of contamination have *not* affected any particular experiment, and deviations from predicted values, as shown for instance in Fig. 11a, c, may actually be a good indication for the presence of small amounts of contaminant. Because of this we propose that our predicted values may be more reliable than most of the measured values for the LREE.

Application to mantle melting

Because of the approach we have taken, we are able to make predictions of REE partitioning behaviour lying outside the P–T–X range used for calibration of the model. To illustrate this, we present a new set of partition coefficients applicable to the onset of melting in the garnet stability field of MORB pyrolite. Recently, Robinson and Wood (1998) studied the garnet–spinel transition in MORB pyrolite close to solidus conditions. They concluded that the P–T path that is followed by MORB pyrolite in a mantle with potential temperature of 1,450 °C, crosses the solidus at 3.5 GPa and 1,500 °C. After 3% partial melting, the garnet–spinel transformation is completed (i.e. all garnet in the residue has been

Comparison between predicted and measured garnet-melt partitioning data
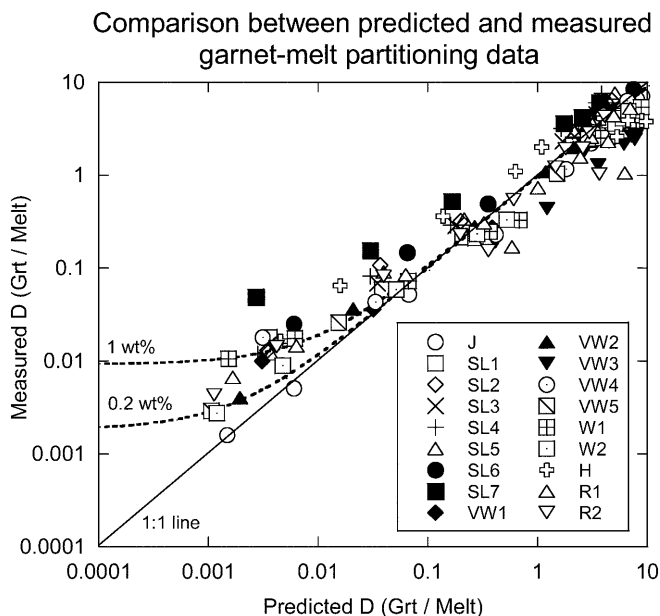
Fig. 12 Measured vs. predicted values of $D^{\mathrm{Grt/Melt}}$ for all available anhydrous garnet–melt partitioning experiments (18 experiments, total number of $D^{\mathrm{Grt/Melt}}$ measurements: 157). Predicted values of r_0, D_0 and E_X are from Eqs. (2), (3) and (29) (Table 2). *J* Johnson (1998); *SL1–7* Salters and Longhi (1999) experiments TM694-3, TM694-6, TM295-4, MO895-1, MO895-2, MO895-3, TM1295-2 respectively; *VW1–3* Van Westrenen et al. (1999a) experiments 8, 11, 13 respectively; *VW4–5* Van Westrenen et al. (2000b), experiments 16, 18; *W1–2* Withers (1997), experiments AOB1.08, AOB1.11; *H* Hauri et al. (1994); *R1–2* Rocholl et al. (1996), experiments 829, 832. *1:1 line* shown for reference. *Dashed lines* show changes in measured $D^{\mathrm{Grt/Melt}}$ by 0.2 and 1 wt% melt addition during garnet analysis

converted to spinel by the reaction grt + ol = sp + opx + cpx) at 2.9 GPa and 1,480 °C. Taking mineral compositions from Robinson and Wood (1998), we can now use Eqs. (2), (3) and (29) to predict $D_0(3+)$, $r_0(3+)$ and $E_X(3+)$ for the melting interval within the garnet stability field. Resulting predictions are given in Table 3. $D_0(3+)$ increases from 15 at 3.5 GPa to 21 at 2.9 GPa, while $r_0(3+)$ increases slightly, with concomitant decrease in $E_X(3+)$. Resulting garnet–melt D_{REE} range from 12 (Lu) to 0.0028 (La) at the onset of melting, and from 17 (Lu) to 0.0044 (La) when the garnet–spinel transformation has been completed. These values are up to 100% higher than values currently used for melting of pyrolite in the garnet stability field (e.g. McKenzie and O'Nions 1991; Spiegelman 1996; Blundy and Brodie 1997).

Conclusions

We have developed a predictive model for the partitioning of trace elements (REE, Y, In and Sc) between garnet and anhydrous silicate melt as a function of pressure, temperature, and garnet and melt composition. The model is based on a combination of the Blundy and Wood (1994) model of partitioning [Eq.

Table 3 Predicted values of *D*(Grt/Melt) during partial melting of MORB pyrolite. *P–T* conditions and garnet major element compositions taken from Robinson and Wood (1998)

Element	D(Grt/Melt)	
	$P = 3.5$ GPa, $T = 1{,}773$ K	$P = 2.9$ GPa, $T = 1{,}753$ K
Sc	7.9	10
Y	5.4	7.5
La	0.0028	0.0044
Ce	0.011	0.017
Pr	0.036	0.055
Nd	0.11	0.16
Sm	0.56	0.82
Eu	1.0	1.5
Gd	1.8	2.5
Tb	2.8	4.0
Dy	4.3	6.1
Ho	5.9	8.3
Er	7.7	11
Tm	9.4	13
Yb	11	15
Lu	12	17

(1)] and a thermodynamic description of the mineral–melt equilibrium for component $JMg_2Al_3Si_2O_{12}$, which explicitly incorporates a measure of garnet non-ideality. Our model reproduces available garnet–melt partitioning data to within 5–50% with the exception of Ce and La, and enables prediction of partition coefficients for any *P–T* condition relevant to anhydrous partial melting of the Earth's upper mantle in the presence of garnet. Important caveats are that our model is only applicable to anhydrous melting, at pressures lower than 7.5 GPa.

References

Baker MB, Hirschmann MM, Ghiorso MS, Stolper EM (1995) Compositions of near-solidus peridotite melts from experiments and thermodynamic calculations. Nature 375:308–311

Barth MG, Foley SF, Horn I (1997) Experimental trace element partitioning in tonalitic systems. LPI Contrib 921:18

Bass JD (1995) Elasticity of minerals, glasses and melts. In: Ahrens TJ (ed) Mineral physics and crystallography – a handbook of physical constants. American Geophysical Union, Washington, DC, pp 45–63

Berman RG (1988) Internally consistent thermodynamic data for stoichiometric minerals in the system Na$_2$O–K$_2$O–CaO–MgO–FeO–Fe$_2$O$_3$–Al$_2$O$_3$–SiO$_2$–TiO$_2$–H$_2$O–CO$_2$. J Petrol 29:445–522

Berman RG (1990) Mixing properties of Ca–Mg–Fe–Mn garnets. Am Mineral 75:328–344

Berman RG, Aranovich LY (1996) Optimized standard state and solution properties of minerals. I. Model calibration for olivine, orthopyroxene, cordierite, garnet, and ilmenite in the system FeO–MgO–CaO–Al$_2$O$_3$–TiO$_2$–SiO$_2$. Contrib Mineral Petrol 126:1–24

Blundy JD, Brodie J (1997) Modelling mantle melting with variable partition coefficients. LPI Contrib 921:30–31

Blundy JD, Dalton J (2000) Experimental comparison of trace element partitioning between clinopyroxene and melt in carbonate and silicate systems, and implications for mantle metasomatism. Contrib Mineral Petrol 139:356–371

Blundy JD, Wood BJ (1994) Prediction of crystal–melt partition coefficients from elastic moduli. Nature 372:452–454

Blundy JD, Wood BJ (1999) The effects of pressure, temperature and melt composition on crystal–melt partitioning of trace elements. EOS Trans Am Geophys Union 80:F1113

Blundy JD, Falloon TJ, Wood BJ, Dalton JA (1995) Sodium partitioning between clinopyroxene and silicate melts. J Geophys Res 100:15501–15515

Blundy JD, Robinson JAC, Wood BJ (1998) Heavy REE are compatible in clinopyroxene on the spinel lherzolite solidus. Earth Planet Sci Lett 160:493–504

Bosenick A, Geiger CA (1997) Powder X-ray diffraction study of synthetic pyrope–grossular garnets between 20 and 295 K. J Geophys Res 102:22649–22657

Bourdon B, Zindler A, Elliott T, Langmuir CH (1996) Constraints on mantle melting at mid-ocean ridges from global ^{238}U–^{230}Th disequilibrium data. Nature 384:231–235

Bowen NL (1913) The melting phenomena of the plagioclase feldspars. Am J Sci 35:577–599

Boyd FR, England JL (1962) Mantle minerals. Carnegie Inst Wash Yearb 61:107–112

Brice JC (1975) Some thermodynamic aspects of the growth of strained crystals. J Cryst Growth 28:249–253

Burnham CW (1981) The nature of multicomponent aluminosilicate melts. Phys Chem Earth 13:197–229

Enami M, Cong B, Yoshida T, Kawabe I (1995) A mechanism for Na incorporation in garnet: an example from garnet in orthogneiss from the Su-Lu terrane, eastern China. Am Mineral 80:475–482

Falloon TJ, Green DH, O'Neill HStC, Hibberson WO (1997) Experimental tests of low degree peridotite partial melt compositions: implications for the nature of anhydrous near-solidus peridotite melts at 1 GPa. Earth Planet Sci Lett 152:149–162

Falloon TJ, Green DH, Danyushevsky LV, Faul UH (1999) Peridotite melting at 1.0 and 1.5 GPa: an experimental evaluation of techniques using diamond aggregates and mineral mixes for determination of near-solidus melts. J Petrol 40:1343–1375

Fratello VJ, Brandle CD (1993) Physical properties of a Y$_3$Al$_5$O$_{12}$ melt. J Cryst Growth 128:1006–1010

Gaetani GA, Grove TL (1998) The influence of water on melting of mantle peridotite. Contrib Mineral Petrol 131:323–346

Ganguly J, Cheng W, O'Neill HStC (1993) Syntheses, volume, and structural changes of garnets in the pyrope–grossular join: implications for stability and mixing properties. Am Mineral 78:583–593

Green TH, Ringwood AE (1968) Genesis of the calc-alkaline igneous rock suite. Contrib Mineral Petrol 18:105–162

Green TH, Blundy JD, Adam J, Yaxley GM (2000) SIMS determination of trace element partition coefficients between garnet, clinopyroxene and hydrous basaltic liquids at 2–7.5 GPa and 1080–1200 °C. Lithos 53:165–189

Gudfinnsson GH, Presnall DC (1996) Melting relations of model lherzolite in the system CaO–MgO–Al$_2$O$_3$–SiO$_2$ at 2.4–3.4 GPa and the generation of komatiites. J Geophys Res 101:27701–27709

Hauri EH, Wagner TP, Grove TL (1994) Experimental and natural partitioning of Th, U, Pb and other trace elements between garnet, clinopyroxene and basaltic melts. Chem Geol 117:149–166

Hazen RM, Finger LW (1979) Bulk modulus–volume relationship for cation–anion polyhedra. J Geophys Res 84:6723–6728

Helffrich G, Wood B (1989) Subregular model for multicomponent solutions. Am Mineral 74:1016–1022

Herzberg C, Zhang J (1997) Melting experiments on komatiite analog compositions at 5 GPa. Am Mineral 82:354–367

Hill E, Wood BJ, Blundy JD (2000) The effect of Ca-Tschermaks component on trace element partitioning between clinopyroxene and silicate melt. Lithos 53:205–217

Hirschmann MM (2000) Mantle solidus: experimental constraints and the effects of peridotite composition. Geochem Geophys Geosys 1:2000GC000070

Hirschmann MM, Stolper EM (1996) A possible role for garnet pyroxenite in the origin of the "garnet signature" in MORB. Contrib Mineral Petrol 124:185–208

Hirschmann MM, Baker MB, Stolper EM (1998) The effects of alkalis on the silica content of mantle-derived melts. Geochim Cosmochim Acta 62:883–902

Irifune T, Ohtani E (1986) Melting of pyrope $Mg_3Al_2Si_3O_{12}$ up to 10 GPa: probability of a pressure-induced structural change in pyrope melt. J Geophys Res 91:9357–9366

Jensen BB (1973) Patterns of trace element partitioning. Geochim Cosmochim Acta 37:2227–2242

Johnson KTM (1998) Experimental determination of partition coefficients for rare earth and high-field-strength elements between clinopyroxene, garnet, and basaltic melt at high pressures. Contrib Mineral Petrol 133:60–68

Johnson KTM, Dick HJB, Shimizu N (1990) Melting in the oceanic upper mantle: an ion microprobe study of diopsides in abyssal peridotites. J Geophys Res 95:2661–2678

Lange RL, Carmichael ISE (1990) Thermodynamic properties of silicate liquids with emphasis on density, thermal expansion and compressibility. Rev Mineral 24:25–64

LaTourrette TZ, Kennedy AK, Wasserburg GJ (1993) Thorium–uranium fractionation by garnet: evidence for a deep source and rapid rise of oceanic basalts. Science 261:739–742

Law KM, Blundy JD, Wood BJ, Ragnarsdottir KV (2000) Trace element partitioning between wollastonite and silicate–carbonate melt. Mineral Mag 64:155–165

Lin I-C, Navrotsky A, Weber JKR, Nordine PC (1999) Thermodynamics of glass formation and metastable solidification of molten $Y_3Al_5O_{12}$. J Non-Cryst Solids 243:273–276

Longhi J (1995) Liquidus equilibria of some primary lunar and terrestrial melts in the garnet stability field. Geochim Cosmochim Acta 59:2375–2386

Lundstrom CC, Shaw HF, Ryerson FJ, Williams Q, Gill J (1998) Crystal chemical control of clinopyroxene–melt partitioning in the Di–Ab–An system: implications for elemental fractionations in the depleted mantle. Geochim Cosmochim Acta 62:2849–2862

Matsui Y, Onuma N, Nagasawa H, Higuchi H, Banno S (1977) Crystal structure control in trace element partition between crystal and magma. Bull Soc Fr Mineral Cristal 100:315–324

McKenzie D, O'Nions RK (1991) Partial melt distributions from inversion of rare earth element concentrations. J Petrol 32:1021–1091

Mukhopadhyay B, Holdaway MJ, Koziol AM (1997) A statistical model of thermodynamic mixing properties of Ca–Mg–Fe^{2+} garnets. Am Mineral 82:165–181

Newton RC, Charlu TV, Kleppa OJ (1977) Thermochemistry of high pressure garnets and clinopyroxenes in the system CaO–MgO–Al_2O_3–SiO_2. Geochim Cosmochim Acta 41:369–377

Nicholls IA, Harris KL (1980) Experimental rare earth element partition coefficients for garnet, clinopyroxene and amphibole coexisting with andesitic and basaltic liquids. Geochim Cosmochim Acta 44:287–308

Ohtani E, Kawabe I, Moriyama J, Nagata Y (1989) Partitioning of elements between majorite garnet and melt and implications for petrogenesis of komatiite. Contrib Mineral Petrol 103:263–269

O'Reilly SY, Griffin WL (1995) Trace-element partitioning between garnet and clinopyroxenes in mantle-derived pyroxenites and eclogites: P–T–X controls. Chem Geol 121:105–130

Patiño Douce AE, Beard JS (1995) Dehydration–melting of biotite gneiss and quartz amphibolite from 3 to 15 kbar. J Petrol 36:707–738

Philpotts JA (1978) The law of constant rejection. Geochim Cosmochim Acta 42:909–920

Putirka K (1998) Garnet + liquid equilibrium. Contrib Mineral Petrol 131:273–288

Putirka K (1999) Melting depths and mantle heterogeneity beneath Hawaii and the East Pacific Rise: constraints from Na/Ti and rare earth element ratios. J Geophys Res 104:2817–2829

Rapp RP (1995) Amphibole-out phase boundary in partially melted metabasalt, its control over liquid fraction and composition, and source permeability. J Geophys Res 100:15601–15610

Rapp RP, Watson EB (1995) Dehydration melting of metabasalt at 8–32 kbar: implications for continental growth and crust–mantle recycling. J Petrol 36:891–931

Rapp RP, Shimizu N, Norman MD, Applegate GS (1999) Reaction between slab-derived melts and peridotite in the mantle wedge: experimental constraints at 3.8 GPa. Chem Geol 160:335–356

Ray GL, Shimizu N, Hart SR (1983) An ion microprobe study of the partitioning of trace elements between clinopyroxene and liquid in the system diopside–albite–anorthite. Geochim Cosmochim Acta 47:2131–2140

Robie RA, Hemingway BS (1995) Thermodynamic properties of minerals and related substances. US Geol Surv Bull 2131:60

Robinson JAC, Wood BJ (1998) The depth of the garnet/spinel transition in fractionally melting peridotite. Earth Planet Sci Lett 164:277–284

Robinson JAC, Wood BJ, Blundy JD (1998) The beginning of melting of fertile and depleted peridotite at 1.5 GPa. Earth Planet Sci Lett 155:97–111

Rocholl A, Ludwig T, Altherr R, Meyer H-P, Brey G, Velz S, Seck H-A, Bulatov V (1996) Experimental partitioning of trace elements between clinopyroxene, garnet and basanitic melts studied by ion microprobe. J Conf Abstr 1:517–518

Salters VJM, Hart SR (1989) The hafnium paradox and the role of garnet in the source of mid-ocean-ridge basalts. Nature 342:420–422

Salters VJM, Longhi J (1999) Trace element partitioning during the initial stages of melting beneath mid-ocean ridges. Earth Planet Sci Lett 166:15–30

Sen C, Dunn T (1994) Dehydration melting of a basaltic composition amphibolite at 1.5 and 2.0 GPa: implications for the origin of adakites. Contrib Mineral Petrol 117:394–409

Shen G, Lazor P (1995) Measurement of melting temperatures of some minerals under lower mantle pressures. J Geophys Res 100:17699–17713

Spiegelman M (1996) Geochemical consequences of melt transport in 2-D: the sensitivity of trace elements to mantle dynamics. Earth Planet Sci Lett 139:115–132

Stracke A, Salters VJM, Sims KWW (1999) Assessing the presence of garnet–pyroxenite in the mantle sources of basalts through combined hafnium–neodymium–thorium isotope systematics. Geochem Geophys Geosys 1:1999GC000013

Takahashi E (1986) Melting a dry peridotite KLB-1 up to 14 GPa: implications on the origin of peridotitic upper mantle. J Geophys Res 91:9367–9382

Téqui C, Robie RA, Hemingway BS, Neuville DR, Richet P (1991) Melting and thermodynamic properties of pyrope ($Mg_3Al_2Si_3O_{12}$). Geochim Cosmochim Acta 55:1005–1010

Trønnes RG, Canil D, Wei K (1992) Element partitioning between silicate minerals and coexisting melts at pressures of 1–27 GPa, and implications for mantle evolution. Earth Planet Sci Lett 111:241–255

Turner S, Blundy J, Wood BJ, Hole M (2000) Large ^{230}Th-excesses in basalts produced by partial melting of spinel lherzolite. Chem Geol 162:127–136

Van Westrenen W, Blundy JD, Wood BJ (1999a) Crystal-chemical controls on trace element partitioning between garnet and anhydrous silicate melt. Am Mineral 84:838–847

Van Westrenen W, Blundy JD, Wood BJ (1999b) Prediction of garnet–silicate melt trace element partition coefficients. EOS Trans Am Geophys Union 80:S357

Van Westrenen W, Allan NL, Blundy JD, Purton JA, Wood BJ (2000a) Atomistic simulation of trace element incorporation

234

into garnets – comparison with experimental garnet–melt partitioning data. Geochim Cosmochim Acta 64:1629–1639

Van Westrenen W, Blundy JD, Wood BJ (2000b) Effect of Fe^{2+} on garnet–melt trace element partitioning: experiments in FCMAS and quantification of crystal-chemical controls in natural systems. Lithos 53:191–203

Van Westrenen W, Blundy JD, Wood BJ (2001) High field strength element/rare earth element fractionation during partial melting in the presence of garnet: implications for identification of mantle heterogeneities. Geochem Geophys Geosys 2:2000GC000133

Walter MJ (1998) Melting of garnet peridotite and the origin of komatiite and depleted lithosphere. J Petrol 39:29–60

Walter MJ, Presnall DC (1994) Melting behavior of simplified lherzolite in the system $CaO–MgO–Al_2O_3–SiO_2–Na_2O$ from 7 to 35 kbar. J Petrol 35:329–359

Webb SL (1989) The elasticity of the upper mantle silicates olivine and garnet to 3 GPa. Phys Chem Mineral 16:684–692

Withers AC (1997) Water in the mantle. PhD Thesis, University of Bristol, UK

Wolf MB, Wyllie PJ (1994) Dehydration–melting of amphibolite at 10 kbar: the effects of temperature and time. Contrib Mineral Petrol 115:369–383

Wood BJ (1988) Activity measurements and excess entropy–volume relationships for pyrope–grossular garnets. J Geol 96:721–729

Wood BJ, Blundy JD (1997) A predictive model for rare earth element partitioning between clinopyroxene and anhydrous silicate melt. Contrib Mineral Petrol 129:166–181

Wood BJ, Fraser DG (1976) Elementary thermodynamics for geologists. Oxford University Press, Oxford

Wood BJ, Blundy JD, Robinson JAC (1999) The role of clinopyroxene in generating U-series disequilibrium during mantle melting. Geochim Cosmochim Acta 63:1613–1620

Yasuda A, Fujii T, Kurita K (1994) Melting phase relations of an anhydrous mid-ocean ridge basalt from 3 to 20 GPa: implications for the behavior of subducted oceanic crust in the mantle. J Geophys Res 99:9401–9414

Zhang J, Herzberg C (1994) Melting of pyrope, $Mg_3Al_2Si_3O_{12}$, at 7–16 GPa. Am Mineral 79:497–503